

MOLECULAR ABUNDANCES IN THE HIGH-LATITUDE MOLECULAR CLOUDS

LORIS MAGNANI¹

E. O. Hulburt Center for Space Research, Naval Research Laboratory; and University of Maryland

LEO BLITZ²

University of Maryland

AND

JAN G. A. WOUTERLOOT

Max-Planck-Institut für Radioastronomie

Received 1987 May 18; accepted 1987 August 3

ABSTRACT

The abundances of CO, OH, and H₂CO are determined for a sample of high-latitude molecular clouds. In spite of the low average extinction of these objects ($A_v \sim 0.6$ mag), which is similar to the extinction in the diffuse molecular clouds identified via UV absorption lines, the high-latitude clouds show abundances similar to those of the dark molecular clouds, where the gas phase chemistry is substantially different. In particular, the CO abundance with respect to H₂ ($[4-12] \times 10^{-5}$) is consistent with abundance determinations in dark clouds ($[5-10] \times 10^{-5}$), the H₂CO abundance is $\sim(2-3) \times 10^{-9}$, consistent with the dark cloud value, and the OH abundance is $\sim 2 \times 10^{-6}$, a factor of 10 greater.

The correlation between the integrated CO antenna temperature and the visual extinction for the high-latitude clouds is poor if the two dark molecular clouds present in the sample are excluded. The $N(\text{H}_2)/W_{\text{CO}}$ ratio is determined from the CO and extinction data and produces a weighted average of 3.2×10^{20} molecules $\text{cm}^{-2} \text{K}^{-1} (\text{km s}^{-1})^{-1}$. However, individual cloud values range from 1×10^{20} to 6×10^{20} molecules $\text{cm}^{-2} \text{K}^{-1} (\text{km s}^{-1})^{-1}$ so that there exists a real variation in the $N(\text{H}_2)/W_{\text{CO}}$ ratio from object to object.

Possible explanations for the enhanced molecular abundances in the high-latitude clouds with respect to the diffuse molecular clouds include decreased levels of photodissociation due to a reduced ambient UV radiation field or increased molecular production by nondissociative shocks.

Subject headings: interstellar: abundances — interstellar: molecules

I. INTRODUCTION

The molecular component of the interstellar medium (ISM) has been subdivided into several categories depending principally on the size or density of the structures. Giant molecular clouds (GMCs), molecular clouds, dark dust clouds, and diffuse molecular clouds are some of the more common categories, with no clear-cut quantitative discriminant between them (i.e., between small GMCs and large molecular clouds). The CO($J = 1-0$) antenna temperatures and line widths in the high-latitude molecular clouds (Magnani, Blitz, and Mundy 1985, hereafter MBM) have values similar to those in the outer regions of dark dust clouds (e.g., Dickman 1975), but the low visual extinctions averaged over a cloud (0.3–0.9 mag) are similar to the extinctions in diffuse molecular clouds (e.g., Savage *et al.* 1977). There are significant differences in the molecular abundances in dark and diffuse molecular clouds because the gas phase chemistry is very sensitive to the interstellar UV radiation field and thus to the extinction in a cloud (e.g., Viala 1986). Specifically, the $N(\text{CO})/N(\text{H}_2)$ ratio in dark clouds has typical values of $\sim 5 \times 10^{-5}$ (Frerking, Langer, and Wilson 1982; Williams 1985), while, for diffuse molecular clouds, values for the ratio vary, but they are typically 2 orders of magnitude lower (e.g., Williams 1985, and references therein). One of the goals of this work is to determine whether the high-latitude clouds are classified more appropriately as dark or as diffuse clouds.

This paper presents CO, H₂CO, OH, and extinction data for several high-latitude molecular clouds in an attempt to determine the molecular abundances and gas properties of a “typical” high-latitude cloud. Section II describes the observational techniques and data reduction procedures and § III presents the results of the observations. The analysis and correlations between the observed and the derived quantities are discussed in § IV, and a short summary of the paper is presented in § V.

II. OBSERVATIONS AND DATA REDUCTION

a) OH

The OH observations were made with the 43 m (140 foot) telescope at the National Radio Astronomy Observatory³ (NRAO) in Green Bank, West Virginia during 1985 April. The front end consisted of dual-channel cooled field effect transistor (FET) amplifiers with a single beam feed that yields orthogonal linear polarizations. The spectrometer was a Mark II autocorrelator split into four receivers of 128 channels each. All four ground-state 18 cm OH lines (1612, 1665, 1667, and 1720 MHz) were observed simultaneously. However, terrestrial interference prevented detection of the 1612 MHz line.

The total system temperature at the zenith for the observations was typically 23–25 K. The bandwidth for the observations covered $\pm 28 \text{ km s}^{-1}$, centered on zero velocity with

¹ NRL–NRC Cooperative Research Fellow.

² Alfred P. Sloan Foundation Fellow.

³ The National Radio Astronomy Observatory is operated by Associated Universities, Inc., under contract with the National Science Foundation.

respect to the LSR and with a resolution per channel of 0.44 km s^{-1} . The OH data were obtained in the frequency switching mode; the reference was switched by an amount equal to the bandwidth. The angular resolution of the observations was $\sim 18'$.

b) H_2CO

The 4830 MHz H_2CO absorption line was observed in 1985 June, July, and December with the 100 m telescope (beam size $2'9''$ at 6 cm) at Effelsberg, West Germany. Only the high-latitude clouds with relatively high CO antenna temperatures in the regions of peak emission ($T_A^* \geq 3 \text{ K}$) were observed. A cooled paramp receiver (system temperature 35 K) and a 1024 channel autocorrelator split into two equal parts were used. The observations were made simultaneously with bandwidths of 3125 and 781 kHz (velocity resolution 0.38 and 0.09 km s^{-1} , respectively) in the frequency switching mode with the expected signal situated in both signal and reference band and with an integration time of 30 minutes. The spectra were folded, and the resulting rms noise was 0.02 K in the low-resolution spectra and 0.04 K in the high-resolution spectra.

The core regions of clouds 7 and 55 were mapped in a square grid pattern with a beam spacing of 2.5.

c) CO and ^{13}CO

The $\text{CO}(J=1-0)$ and $^{13}\text{CO}(J=1-0)$ data were obtained using the Millimeter Wave Observatory (MWO)⁴ 5 m telescope near Fort Davis, Texas in 1984 and 1985 and with the NRAO 12 m telescope at Kitt Peak during 1985 May. The observing procedure at Texas is as described in MBM.

The NRAO data were obtained using two receivers which detect orthogonal polarizations. The output from one of the receivers was split into two filter banks, a 256 channel, 100 kHz

per channel filter bank and a 128 channel, 30 kHz per channel filter bank. The other polarization was fed to a second 256 channel, 100 kHz per channel filter bank. For the CO observations, the signals in the two 100 kHz banks were combined, resulting in rms noise of $\sim 0.4 \text{ K}$ per channel, while the 30 kHz filter bank produced an rms noise of $\sim 1.3 \text{ K}$ per channel. The ^{13}CO observations were integrated for longer periods of time, resulting in an rms noise in the 100 kHz filters of $\sim 0.15 \text{ K}$. The CO data were obtained in a position-switched mode using reference positions determined from the contour maps in MBM.

At the MWO, the CO antenna temperature is uncorrected for the spillover and scattering efficiency (η_{FSS}) and for the antenna coupling efficiency (η_c). We use $\eta_{\text{FSS}}\eta_c \sim 0.8$ (Lee Mundy, private communication) to convert T_A^* to T_R^* (see Kutner and Ulich 1981). At the NRAO 12 m telescope, the data are obtained as T_R^* . Because the source sizes are greater than a few arcminutes, $\eta_c \sim 1$ (Phil Jewell, private communication). The uncertainty in T_R^* for both sets of data is estimated to be $\sim 15\%$ from observations of standard calibrators.

d) Extinction

The extinction maps and data reduction procedures for the seven high-latitude regions studied are presented in Magnani and de Vries (1986). For the seven molecular complexes, the visual extinction averaged over the area within the lowest $\text{CO}(J=1-0)$ integrated antenna temperature contour (1.0 K km s^{-1}) ranges from 0.3 to 0.9 mag, with an average over the clouds of ~ 0.6 mag. The resolution of the extinction data is $\sim 8'$ and the relative uncertainty in visual extinction for each line of sight $\Delta A_v/A_v$ is $\sim 70\%$.

III. RESULTS

a) OH

The line parameters for three of the main OH lines are shown in Table 1. Column (1) gives the cloud number from the MBM catalog, and columns (2) and (3) give the positions of the

TABLE 1
OH OBSERVATIONS—NRAO 43 m GREEN BANK

| CLOUD (1) | α (1950) (2) | δ (1950) (3) | 1665 MHz | | | 1667 MHz | | | 1720 MHz | | |
|--------------|---|---------------------------|---------------------|---|---|---------------------|---|---|----------------------|--|--|
| | | | T_B (K) (4) | Δv (km s^{-1}) (5) | v_{LSR} (km s^{-1}) (6) | T_B (K) (7) | Δv (km s^{-1}) (8) | v_{LSR} (km s^{-1}) (9) | T_B (K) (10) | Δv (km s^{-1}) (11) | v_{LSR} (km s^{-1}) (12) |
| 6..... | 2 ^h 01 ^m 06 ^s .0 | 20°09'00" | 0.047 | 0.98 | 6.48 | 0.078 | 1.07 | 6.74 | | | rms = 0.014 |
| 7..... | 2 19 35.9 | 19 40 00 | 0.038 | 1.53 | 5.27 | 0.071 | 1.02 | 4.98 | | | rms = 0.016 |
| 16..... | 3 16 20.0 | 11 24 00 | 0.052 | 2.23 | 6.91 | 0.074 | 1.83 | 6.71 | | | rms = 0.016 |
| | 3 17 42.0 | 10 30 00 | 0.091 | 1.34 | 7.38 | 0.134 | 1.69 | 7.22 | 0.044 | 1.55 | 7.66 |
| 20..... | 4 32 44.7 | -14 19 36 | 0.246 | 0.54 | 0.24 | 0.330 | 0.78 | 0.23 | 0.098 | 0.77 | 0.25 |
| 21..... | 4 59 24.0 | -9 00 00 | 0.067 | 0.82 | 4.69 | 0.055 | 0.97 | 4.79 | 0.039 | 1.02 | 4.99 |
| 22..... | 5 02 12.0 | -8 20 00 | | rms = 0.026 | | | rms = 0.022 | | | | rms = 0.026 |
| 26..... | 8 02 47.9 | 60 43 00 | 0.038 | 0.58 | -0.64 | 0.041 | 1.36 | -1.05 | | | rms = 0.017 |
| 28..... | 8 52 48.0 | 72 28 00 | 0.017 | 6.45 | 0.87 | 0.033 | 4.48 | 1.75 | | | rms = 0.011 |
| 30..... | 9 24 12.0 | 70 38 00 | 0.243 | 3.21 | 2.68 | 0.374 | 2.60 | 2.13 | | | rms = 0.017 |
| 32..... | 9 28 42.0 | 66 05 00 | 0.042 | 1.55 | 3.68 | 0.086 | 1.15 | 4.10 | ... | ... | ... |
| 38..... | 15 57 05.8 | -1 32 58 | 0.056 | 0.49 | 0.88 | 0.052 | 0.72 | 0.84 | | | rms = 0.020 |
| 40..... | 16 08 23.9 | 21 56 58 | 0.031 | 0.87 | 3.27 | 0.072 | 1.07 | 3.23 | ... | ... | ... |
| | 16 07 11.8 | 22 15 00 | 0.029 | 1.03 | 2.58 | 0.059 | 0.69 | 2.95 | | | rms = 0.010 |
| 55..... | 23 05 53.9 | 15 07 00 | 0.025 | 2.27 | -9.16 | {0.042 | 2.39 | -9.57 | | | rms = 0.011 |
| | | | | | | {0.020 | 4.20 | -5.63 | | | |
| | | | {0.022 | 0.31 | -9.75 | 0.033 | 1.68 | -9.28 | | | |
| | 23 05 53.9 | 14 49 00 | {0.020 | 3.62 | -7.65 | 0.043 | 2.03 | -7.10 | | | rms = 0.011 |
| | | | {0.018 | 0.44 | -4.47 | 0.026 | 1.29 | -4.76 | | | |

NOTE.—Where no line was detected the rms noise (in K) is given in place of the line parameters.

observed lines of sight in 1950 coordinates. The remaining columns list the antenna temperature, the line width, and the velocity centroid of the Gaussian fitted line profile (or the rms noise if no line was detected) for the 1665, 1667, and 1720 MHz lines.

The high-latitude clouds have antenna temperatures of $\sim 1.7 \times 10^{-2}$ – 3.7×10^{-1} K, in the main OH lines, and they were detected in 15 of the 16 lines of sight toward the cloud cores. The lines of sight which were observed were determined from the CO maps in MBM. The 1720 and 1612 MHz satellite lines were much more difficult to detect with only three detections of the former and no detections of the latter because of interference.

We note that the lines of sight for clouds 20 and 30 show antenna temperatures in the main lines nearly 1 order of magnitude greater than those observed for the other high-latitude clouds. Calculations (§ IVb[ii]) show that these two lines of sight have greater excitation temperatures than do the other

lines of sight. However, the derived column densities in these directions are not remarkable compared to those of other lines of sight. Higher resolution mapping of these two regions is required to study the excitation conditions.

b) H₂CO

The results of the 6 cm H₂CO observations for 14 high-latitude clouds are presented in Table 2 and in Figures 1 and 2, the first three columns in Table 2 show the cloud number and the observed line of sight in 1950 coordinates, while the next three columns list the brightness temperature, the FWHM, and the Gaussian fitted velocity centroid of the line. In columns (7) and (8), the antenna temperature and line width of the CO(*J* = 1–0) line are listed if CO data for the line of sight are available. The 6 cm H₂CO transition was detected in absorption for 49 out of 81 lines of sight toward the core regions of the sampled high-latitude clouds.

The core regions of clouds 7 and 55 were mapped in the 6 cm

TABLE 2
H₂CO OBSERVATIONS—MPI 100 m EFFELSBURG

| CLOUD (1) | α (1950) (2) | δ (1950) (3) | H ₂ CO | | | CO(<i>J</i> = 1–0) | |
|--------------|---|---------------------------|---------------------|--|---|-----------------------|--|
| | | | T_B (K) (4) | Δv (km s ⁻¹) (5) | v_{LSR} (km s ⁻¹) (6) | T_A^* (K) (7) | Δv (km s ⁻¹) (8) |
| 6..... | 02 ^b 01 ^m 06 ^s 0 | 20°09'00" | –0.28 | 1.1 | +6.62 | 5.8 | 2.10 |
| 7..... | 02 21 00.0 | 19 20 00 | –0.15 | 0.8 | +4.24 | 5.8 | 1.00 |
| 11..... | 02 48 18.0 | 19 20 00 | | rms = 0.04 | | 4.1 | 0.70 |
| 12..... | 02 54 00.0 | 19 20 00 | –0.33 | 1.2 | –5.53 | 5.7 | 1.69 ^a |
| 16..... | 03 16 09.8 | 11 20 00 | | rms = 0.03 | | ... | ... |
| | 03 16 20.0 | 11 22 30 | | rms = 0.03 | | ... | ... |
| | 03 16 20.0 | 11 20 00 | –0.15 | 0.4 ^b | +7.42 | 4.2 | 0.88 |
| | 03 16 20.0 | 11 17 30 | –0.08 | 1.4 ^b | +7.82 | ... | ... |
| | 03 16 30.2 | 11 20 00 | –0.12 | 0.4 ^b | +7.64 | ... | ... |
| | 03 20 20.0 | 10 40 00 | –0.08 | 1.5 ^b | +6.46 | 4.2 | 0.93 |
| | 03 21 00.0 | 12 20 00 | | rms = 0.03 | | ... | ... |
| 18..... | 03 57 40.0 | 00 00 00 | | rms = 0.04 | | ... | ... |
| | 03 59 40.0 | 01 10 00 | –0.18 | 0.5 | +7.71 | ... | ... |
| | 03 59 50.0 | 01 12 30 | –0.12 | 0.6 | +7.84 | ... | ... |
| | 03 59 50.0 | 01 10 00 | –0.15 | 0.7 | +7.89 | 7.0 | 1.03 |
| | 03 59 50.0 | 01 07 30 | –0.19 | 0.6 | +7.68 | ... | ... |
| | 04 00 00.0 | 01 10 00 | –0.11 | 0.7 | +8.00 | ... | ... |
| 26..... | 08 04 00.0 | 61 22 00 | –0.04 | 5.3 ^b | +0.17 | 2.7 | 0.96 |
| 27..... | 08 43 48.0 | 72 48 00 | | rms = 0.03 | | 3.0 | 0.90 |
| 28..... | 08 52 48.0 | 72 28 00 | | rms = 0.03 | | 3.0 | 1.30 |
| 32..... | 09 28 42.0 | 66 05 00 | | rms = 0.03 | | 4.0 | 1.30 |
| | 09 32 00.0 | 66 05 00 | –0.08 | 1.7 ^b | –0.17 | ... | ... |
| 40..... | 16 08 15.9 | 21 59 48 | –0.08 | 0.7 | +2.84 | ... | ... |
| | 16 08 13.2 | 21 59 30 | –0.08 | 1.2 | +2.83 | 5.7 | 0.54 ^c |
| | 16 08 24.0 | 21 57 00 | –0.07 | 2.4 | +3.77 | 4.4 | 1.01 |
| 53..... | 23 05 40.0 | 22 40 00 | | rms = 0.02 | | ... | ... |
| 55..... | 23 05 30.0 | 14 20 00 | | rms = 0.02 | | ... | ... |
| | 23 05 39.3 | 14 50 00 | | rms = 0.02 | | ... | ... |
| | 23 06 00.0 | 14 55 00 | | rms = 0.02 | | 1.9 | 3.14 |
| | 23 06 00.0 | 14 50 00 | –0.09 | 3.9 ^b | –7.96 | ... | ... |
| | 23 06 00.0 | 14 45 00 | | rms = 0.02 | | ... | ... |
| | 23 06 00.0 | 14 20 00 | –0.09 | 0.9 ^b | –7.30 | ... | ... |
| | | | –0.11 | 1.4 ^b | –4.34 | 4.3 | 1.78 |
| | 23 06 20.7 | 14 50 00 | –0.09 | 1.2 ^b | –7.02 | ... | ... |
| 56..... | 23 22 10.0 | 33 05 00 | | rms = 0.03 | | ... | ... |

^a Tabulated CO component at $v = -5.32$ km s⁻¹; another component with $T_A^* = 2.4$ K, $\Delta v = 1.65$ km s⁻¹, at $v = +0.04$ km s⁻¹.

^b Resolution is 0.4 km s⁻¹; all other entries at 0.1 km s⁻¹ resolution.

^c Tabulated CO component at $v = +3.52$ km s⁻¹; another component with $T_A^* = 1.2$ and $\Delta v = 1.11$ km s⁻¹ at $v = +4.08$ km s⁻¹.

NOTE.—Where no line was detected the rms noise (in K) is given in place of the line parameters.

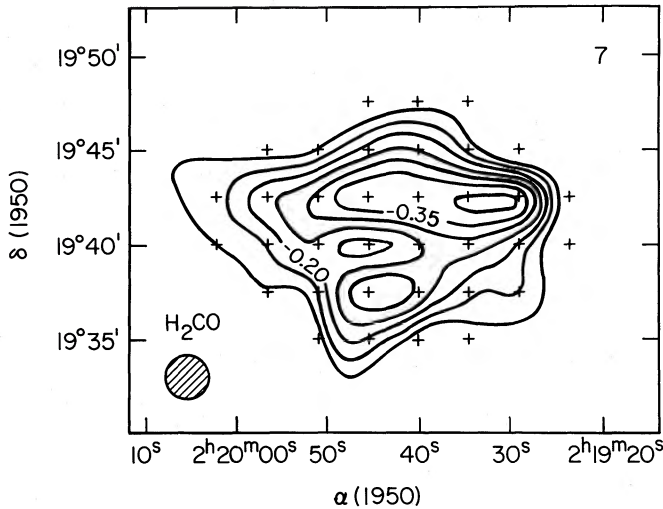


FIG. 1a

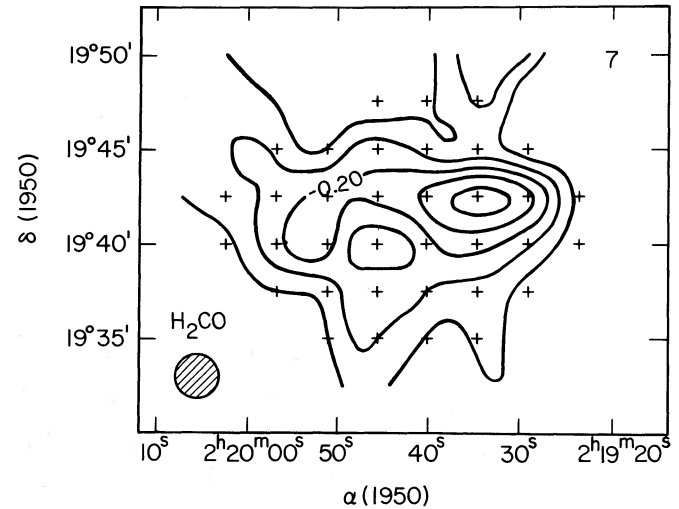


FIG. 1b

FIG. 1.—(a) Velocity-integrated H_2CO brightness temperature map of the core region of cloud 7. The highest contour is at $-0.10 \text{ K km s}^{-1}$, with succeeding contours at 0.05 K km s^{-1} intervals. (b) Minimum H_2CO brightness temperature for the same region as in (a). The highest contour is at -0.10 K , with succeeding contours at 0.05 K .

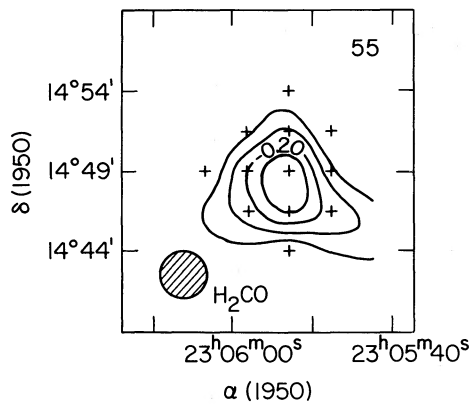


FIG. 2a

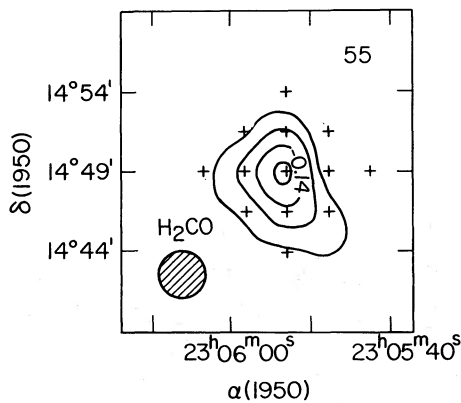


FIG. 2b

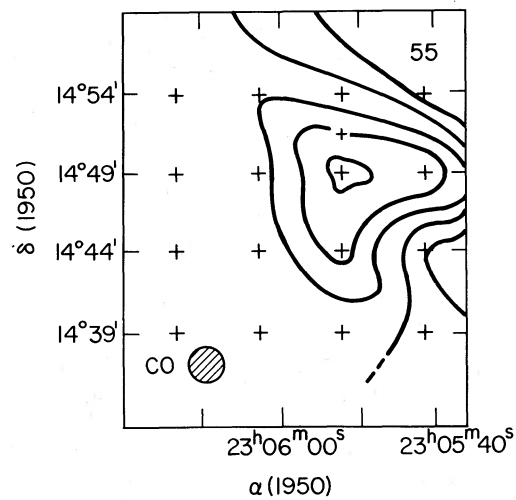


FIG. 2c

FIG. 2.—(a) Velocity-integrated H_2CO brightness temperature map of the core region of cloud 55. The highest contour is at $-0.10 \text{ K km s}^{-1}$, with succeeding contours at 0.05 K km s^{-1} intervals. (b) Minimum H_2CO brightness temperature for the same region as in (a). The highest contour is at -0.08 K , with succeeding contours at 0.03 K intervals. (c) Velocity-integrated CO antenna temperature map of the core region of cloud 55. The area shown is slightly larger than the area in (a) and (b), but is drawn to the same scale. At the resolution of the observations, the entire region exhibits CO emission. The lowest contour shown is at 3 K km s^{-1} , with succeeding contours at 3 K km s^{-1} intervals.

H_2CO transition. In Figure 1a, the integrated H_2CO brightness temperature in K km s^{-1} is displayed, while in Figure 1b the minimum H_2CO brightness temperature (i.e., maximum absorption) for the same region of cloud 7 is displayed. CO data at full beamwidth sampling are not available for cloud 7 at this time, so a direct comparison of the H_2CO absorption and CO emission is not possible.

Figures 2a and 2b show the integrated H_2CO brightness temperature and the minimum H_2CO temperature for one of the core regions of cloud 55. CO data are available for this region and the velocity-integrated CO antenna temperature (W_{CO}) is plotted in Figure 2c on the same scale. Although the CO data are not sampled at full beamwidth resolution, we conclude that in cloud 55 the 6 cm H_2CO absorption line is

detectable at the 0.05 K km s^{-1} level in regions which show a W_{CO} contour greater than 9 K km s^{-1} .

c) CO and ^{13}CO

Table 3 presents the MWO CO($J = 1-0$) and ^{13}CO ($J = 1-0$) data. The first three columns list the cloud number and position in 1950 coordinates, the next three columns show the antenna temperature, line widths, and Gaussian fitted centroid velocity for the CO emission lines, while in the last three columns the same line parameters are listed for the ^{13}CO transition. Table 4 presents all of the ^{13}CO data from the NRAO 12 m telescope (hereafter 12 m data) and the CO data along the corresponding line of sight.

IV. ANALYSIS AND DISCUSSION

a) CO and Extinction Correlations

Because H_2 cannot be observed directly in cold dense gas, trace species must be employed to deduce $N(\text{H}_2)$. The relatively high abundance of CO with respect to H_2 makes CO a good molecule for this purpose. An empirical relationship between $N(\text{H}_2)$ and the readily observable quantity W_{CO} has been established for the Orion molecular complex and other large molecular clouds (Bloemen *et al.* 1984) and for GMCs in the galactic plane (Bloemen *et al.* 1986) using CO, H I, and gamma-ray data. In light of this relationship, W_{CO} is often utilized for determining $N(\text{H}_2)$ in studies of the molecular content of interstellar clouds.

The extinction is also used to determine the hydrogen nucleon content of interstellar clouds. Bohlin, Savage, and Drake (1978) show that, for regions with $A_v < 2$ mag, the extinction is a good tracer of $N(\text{H I}) + 2N(\text{H}_2)$. Correlations of observed quantities such as W_{CO} and A_v and of derived quantities such as $N(\text{CO})$ and $N(\text{H}_2)$ are described in this section, and are summarized in Table 5.

Section IVa (i) discusses the correlation between $N(^{13}\text{CO})$ and A_v , with $N(^{13}\text{CO})$ derived from LTE assumptions and A_v converted to $N(\text{H}_2)$ via the Bohlin, Savage, and Drake (1978)

relation and various assumptions about the $N(\text{H I})$ contribution. A good correlation between W_{CO} and $N(\text{CO})$ is established in § IVa(ii) with the aim of replacing $N(\text{CO})$ in the analysis with the more easily obtained W_{CO} . In § IVa(iii) the two observed quantities W_{CO} and A_v are compared, and A_v is converted to $N(\text{H}_2)$ in order to determine the $N(\text{H}_2)/W_{\text{CO}}$ ratio for the high-latitude clouds.

Sections IVb(i)–IVb(iii) discuss the CO, OH, and H_2CO abundances in the high-latitude clouds. The abundances are much higher than those determined from UV observations of diffuse molecular clouds and more closely resemble abundances in dark molecular clouds. Two possible causes for the high molecular abundances in these objects, a reduced ambient UV radiation field and nondissociative shocks, are described in §§ IVb(iv) and IVb(v).

The differences in sampling and resolution between the extinction data and the CO data (8' sampling and resolution for A_v ; 10'–20' sampling and 2.3 resolution for CO) should be kept in mind throughout the following discussion. Depending on how clumpy the high-latitude clouds are, the extinction averaged over an area 8' in diameter could, in principle, underestimate the true extinction arising solely from a smaller clump within the area used to obtain the extinction. Although the CO beam size is only 2.3, the sampling size is generally about 10', close to the resolution of the extinction pixels. If the extinction arises solely from the CO-emitting region, we would expect that sometimes the CO sampled point within the extinction pixel would imply the presence of less CO than the "true" amount in the 8' pixel. This would tend to overestimate by a factor of a few the conversion factor from W_{CO} to $N(\text{H}_2)$. However, since the star counts are statistical and even the smallest cloud for which we have extinction data has at least 60 extinction pixels within the lowest MBM CO boundary, the overestimate of $N(\text{H}_2)/W_{\text{CO}}$ should be compensated for by the values from extinction pixels that comprise regions where the CO sampled emission underestimates the CO contribution. Thus, although in principle our CO/ H_2 conversions may be in error by as much as a factor of 2 or 3 due to the different

TABLE 3^a
CO AND ^{13}CO OBSERVATIONS—5 m MWO

| CLOUD (1) | α (1950) (2) | δ (1950) (3) | CO($J = 1-0$) | | | ^{13}CO ($J = 1-0$) | | |
|--------------|---|---------------------------|-----------------------|--|---|--------------------------------|--|---|
| | | | T_A^* (K) (4) | Δv (FWHM) (km s^{-1}) (5) | v_{LSR} (km s^{-1}) (6) | T_A^* (K) (7) | Δv (FWHM) (km s^{-1}) (8) | v_{LSR} (km s^{-1}) (9) |
| 40..... | 16 ^h 08 ^m 02 ^s | 22°02'0" | 4.4 | 0.7 | 3.64 | 1.0 | 0.6 | 3.64 |
| | 16 08 13 | 22 04.5 | 6.9 | 0.7 | 3.52 | 1.9 | 0.4 | 3.57 |
| | 16 08 24 | 21 57.0 | 4.7 | 1.0 | 3.87 | 0.7 | 0.9 | 3.81 |
| | 16 08 35 | 21 54.5 | 6.1 | 1.0 | 3.81 | 2.4 | 0.5 | 3.76 |
| | 16 08 13 | 22 02.2 | 6.9 | 0.7 | 3.55 | 1.6 | 0.5 | 3.54 |
| | 16 08 24 | 21 59.5 | 6.6 | 0.6 | 3.66 | 1.0 | 0.5 | 3.66 |
| | 16 08 46 | 21 54.5 | 6.9 | 0.8 | 3.77 | 1.5 | 0.5 | 3.68 |
| | 16 08 46 | 21 52.0 | 6.7 | 1.0 | 3.77 | 1.5 | 0.5 | 3.67 |
| | 16 08 02 | 21 59.5 | 2.7 | 1.0 | 3.60 | 0.3 | 0.7 | 3.53 |
| | 16 08 14 | 21 59.5 | 1.2 | 0.9 | 4.08 | ... | ... | ... |
| | | | 5.7 | 0.5 | 3.52 | 1.0 | 0.4 | 3.59 |
| 53..... | 23 00 00 | 24 37.0 | 1.7 | 0.9 | -4.03 | 0.3 | 0.5 | -3.92 |
| | 23 05 43 | 22 37.0 | 2.3 | 1.1 | -3.17 | 0.2 | 1.4 | -3.11 |
| 55..... | 23 05 54 | 14 39.0 | 1.9 | 2.9 | -7.69 | 0.3 | 1.3 | -7.63 |
| | 23 05 54 | 14 49.0 | 5.2 | 3.0 | -7.36 | 1.5 | 1.6 | -7.18 |
| | 23 06 14 | 14 49.0 | 1.3 | 1.6 | -4.76 | ... | ... | ... |
| | | | 2.2 | 2.0 | -7.36 | 0.2 | 1.6 | -7.63 |

^a Other CO and ^{13}CO MWO observations are presented in MBM.

TABLE 4
CO AND ^{13}CO OBSERVATIONS—12 m NRAO

| CLOUD (1) | α (1950) (2) | δ (1950) (3) | CO($J = 1-0$) | | | $^{13}\text{CO}(J = 1-0)$ | | |
|-----------------------|---|---------------------------|-----------------------|---|---|---------------------------|---|---|
| | | | T_R^* (K) (4) | Δv (km s^{-1}) (5) | v_{LSR} (km s^{-1}) (6) | T_R^* (K) (7) | Δv (km s^{-1}) (8) | v_{LSR} (km s^{-1}) (9) |
| 26 ^a | 08 ^b 02 ^m 21 ^s | 61°26.5 | 5.3 | 0.9 | -0.42 | 1.3 | 0.8 | -0.97 |
| | | | 2.6 | 0.8 | 1.33 | ... | ... | ... |
| | 08 02 30 | 61 26.5 | 4.6 | 1.3 | -0.48 | 1.0 | 0.7 | -0.61 |
| | 08 02 38 | 61 26.5 | 3.7 | 1.2 | -0.36 | 0.8 | 0.6 | -0.35 |
| | 08 02 46 | 61 26.5 | 4.6 | 1.0 | -0.49 | 0.6 | 0.8 | -0.24 |
| | 08 02 55 | 61 26.5 | 4.8 | 1.1 | -0.20 | 0.3 | 1.1 | -0.11 |
| | 08 02 30 | 61 27.5 | 3.8 | 0.9 | -0.29 | 0.7 | 0.6 | -0.42 |
| | 08 02 30 | 61 28.5 | 4.4 | 1.2 | -0.15 | 0.5 | 0.9 | -0.14 |
| | 08 02 38 | 61 28.5 | 3.3 | 1.0 | -0.02 | 0.3 | 1.8 | -0.22 |
| | 08 02 46 | 61 28.5 | 1.9 | 2.7 | -0.40 | 0.5 | 1.2 | +0.22 |
| 08 03 03 | 61 28.5 | 3.3 | 1.5 | -0.31 | 0.3 | 1.5 | +0.21 | |
| 32 ^a | 09 28 12 | 66 09.0 | 3.9 | 1.1 | +3.87 | 0.8 | 0.8 | +4.02 |
| | 09 28 22 | 66 09.0 | 5.1 | 1.2 | +4.29 | 2.0 | 0.8 | +4.18 |
| | 09 28 32 | 66 09.0 | 5.0 | 0.8 | +4.13 | 1.9 | 0.7 | +4.26 |
| | 09 28 42 | 66 09.0 | 5.3 | 0.9 | +4.04 | 1.8 | 0.7 | +4.22 |
| 40 ^b | 16 08 11 | 22 01.0 | 7.4 | 0.6 | +3.06 | 2.4 | 0.3 | +3.19 |
| | 16 08 15 | 22 01.0 | 9.9 | 0.6 | +3.04 | 3.0 | 0.4 | +3.17 |
| | 16 08 19 | 22 01.0 | 8.4 | 0.6 | +3.13 | 2.3 | 0.3 | +3.21 |
| | 16 08 24 | 22 01.0 | 9.2 | 0.5 | +3.08 | 2.1 | 0.4 | +3.19 |
| | 16 08 11 | 22 02.0 | 6.7 | 0.7 | +3.08 | 3.5 | 0.3 | +3.18 |
| | 16 08 15 | 22 02.0 | 7.2 | 0.7 | +3.09 | 3.2 | 0.4 | +3.14 |
| | 16 08 19 | 22 02.0 | 7.3 | 0.6 | +3.10 | 2.2 | 0.5 | +3.14 |
| | 16 08 24 | 22 02.0 | 5.8 | 0.7 | +3.07 | 1.5 | 0.3 | +3.19 |
| | 16 08 28 | 22 02.0 | 4.9 | 0.7 | +3.07 | 0.5 | 0.4 | +3.24 |
| | 55 ^a | 23 05 29 | 14 38.0 | { 3.3 | 1.2 | -8.29 | 0.7 | 1.0 |
| { 1.9 | | | | 1.9 | -5.07 | ... | ... | ... |
| 23 05 34 | | 14 38.0 | { 2.0 | 2.3 | -8.04 | 0.2 | 1.6 | -8.20 |
| | | | { 1.1 | 2.1 | -5.02 | ... | ... | ... |
| 23 05 38 | | 14 38.0 | { 2.1 | 2.0 | -8.29 | 0.6 | 1.2 | -8.14 |
| | | | { 1.5 | 1.8 | -5.42 | ... | ... | ... |
| 23 05 50 | | 14 38.0 | { 1.2 | 1.1 | -9.18 | ... | ... | ... |
| | | | { 1.6 | 5.5 | -6.29 | 0.3 | 2.7 | -6.42 |
| 23 05 38 | | 14 45.0 | 1.3 | 3.0 | -7.06 | 0.4 | 1.3 | -6.94 |
| 25 05 42 | | 14 45.0 | { 2.8 | 0.9 | -7.46 | 1.5 | 0.9 | -7.13 |
| | | | { 1.8 | 2.3 | -6.76 | ... | ... | ... |
| 23 05 46 | | 14 45.0 | { 1.7 | 0.9 | -7.47 | 0.8 | 2.0 | -7.39 |
| | | | { 2.3 | 2.9 | -7.11 | ... | ... | ... |
| 23 05 50 | | 14 45.0 | { 2.5 | 0.7 | -7.76 | 0.7 | 1.4 | -7.46 |
| | | | { 3.4 | 3.0 | -6.93 | ... | ... | ... |
| 23 05 54 | | 14 45.0 | { 3.0 | 1.3 | -7.83 | 1.2 | 1.5 | -7.43 |
| | | | { 2.9 | 2.2 | -6.82 | ... | ... | ... |
| 23 05 58 | | 14 45.0 | { 1.7 | 0.8 | -8.01 | ... | ... | ... |
| | | | { 4.2 | 2.9 | -7.14 | 1.1 | 1.6 | -7.33 |
| 23 06 02 | | 14 45.0 | { 2.7 | 1.3 | -7.79 | ... | ... | ... |
| | | | { 2.0 | 3.1 | -7.22 | 0.5 | 1.7 | -7.27 |
| 23 06 07 | | 14 45.0 | { 1.3 | 1.0 | -8.07 | 0.7 | 0.9 | -7.74 |
| | | | { 3.3 | 2.4 | -7.24 | 0.5 | 0.6 | -6.52 |
| 23 06 11 | | 14 45.0 | { 2.8 | 2.5 | -7.15 | 0.3 | 1.0 | -7.26 |
| | | | { ... | ... | ... | 0.4 | 0.5 | -6.04 |
| 23 06 15 | | 14 45.0 | { 2.8 | 1.7 | -7.39 | 0.5 | 1.0 | -7.15 |
| | | | { 2.1 | 1.0 | -5.79 | 0.5 | 0.5 | -6.13 |
| 23 06 19 | | 14 45.0 | { 3.0 | 2.0 | -7.36 | 0.3 | 1.3 | -6.33 |
| | { 2.1 | | 1.1 | -5.50 | ... | ... | ... | |
| 23 06 23 | 14 45.0 | { 2.9 | 2.1 | -7.62 | 0.3 | 1.1 | -8.29 | |
| | | { 1.3 | 1.2 | -5.58 | 0.3 | 0.5 | -5.43 | |
| 23 06 27 | 14 45.0 | 2.4 | 3.0 | -7.29 | 0.4 | 2.2 | -7.85 | |
| 23 06 31 | 14 45.0 | 2.0 | 2.6 | -6.70 | 0.4 | 1.4 | -6.69 | |

^a Data obtained with 100 kHz resolution, equivalent to 0.26 km s^{-1} per channel.

^b Data obtained with 30 kHz resolution, equivalent to 0.08 km s^{-1} per channel.

TABLE 5
CO, A_v , AND $N(\text{H}_2)$ RELATIONS

| Quantity ^a | Value | Number of Data Points | Remarks |
|---|------------------------------|-----------------------|--|
| 1. $N(\text{H}_{\text{total}})/N(^{13}\text{CO})$ | $3.5 \pm 2.6 \times 10^6$ | 10 | High-latitude clouds |
| 2. $N(\text{H}_{\text{total}})/N(^{13}\text{CO})$ | $1.2 \pm 0.8 \times 10^6$ | 10 | Derived from quantity 1 assuming $N(\text{H}_2) \sim N(\text{H I})$ |
| 3. $N(\text{H}_2)/N(^{13}\text{CO})$ | $3.8 \pm 0.7 \times 10^6$ | 1200 | Derived from Bachiller and Cernicharo 1986 |
| 4. $N(\text{H}_2)/N(^{13}\text{CO})$ | 6.7×10^6 | 8 | Derived from Frerking, Langer, and Wilson 1982 |
| 5. $N(\text{H}_2)/W_{\text{CO}}^b$ | 2.7×10^{20} | ^c | Bloemen <i>et al.</i> 1986 |
| 6. $N(\text{H}_2)/W_{\text{CO}}^b$ | $4.7 \pm 1.1 \times 10^{20}$ | 77 | Dark clouds (Dickman 1978a) |
| 7. $N(\text{H}_2)/W_{\text{CO}}^b$ | 5.5×10^{20} | ~500 | Taurus dark clouds (Wouterloot 1981) |
| 8. $N(\text{H}_2)/W_{\text{CO}}^b$ | $0.5 \pm 0.3 \times 10^{20}$ | ~400 | High-latitude clouds (de Vries, Heithausen, and Thaddeus 1987) |
| 9. $N(\text{H}_2)/W_{\text{CO}}^b$ | $6.4 \pm 1.2 \times 10^{20}$ | 266 | All high-latitude clouds in our sample; based on slope of best-fit line |
| 10. $N(\text{H}_2)/W_{\text{CO}}^b$ | $3.2 \pm 0.1 \times 10^{20}$ | 203 | All high-latitude clouds except dark clouds 18 and 20; based on weighted average |
| 11. $N(\text{H}_2)/W_{\text{CO}}^b$ | $> 1 \times 10^{20}$ | 266 | Lower limit assuming maximum H I contribution. |
| 12. $N(\text{H}_2)/W_{\text{CO}}^b$ | 0.8×10^{20} | 24 | Cloud 20 core $A_v \geq 1.1$ mag |

^a Assuming $N(\text{H}_2) = 9.4 \times 10^{20} A_v \text{ cm}^{-2}$ (Bohlin, Savage, and Drake 1978).

^b In units of molecules $\text{cm}^{-2} \text{K}^{-1} (\text{km s}^{-1})^{-1}$.

^c Based on data from Galactic plane.

resolutions of the data, the central limit theorem makes this possibility unlikely.

In addition, de Vries and Le Poole (1985) and de Vries (1986) report a good correlation between A_v and the *IRAS* 100 μm data for diffuse clouds similar to the ones studied in this paper. For the high-latitude molecular clouds, the 100 μm *IRAS* data show only small relative changes in the 100 μm emissivity on size scales of a few pixels (each *IRAS* pixel at 100 μm is $\sim 2'$ in size). We thus expect that the systematic errors in the quantities derived in § IV a will produce errors of, at most, a factor of 2 from quantities obtained with the same resolution. Such uncertainties will not change the conclusions of the paper.

i) $N(^{13}\text{CO})$ and A_v Correlations

The pioneering work on this subject for a sample of dark clouds is by Dickman (1978a). $N(^{13}\text{CO})$ was obtained for various lines of sight in 38 clouds under the assumption of LTE and then combined with the extinction data to provide an empirical prescription for obtaining $N(\text{H}_2)$. The value quoted by Dickman (1978a), $N(\text{H}_2) = (5.0 \pm 2.5) \times 10^5 N(^{13}\text{CO})$, must be corrected for current A_v to $N(\text{H}_{\text{total}})$ determinations (Bohlin, Savage, and Drake 1978) and for the change in the CO dipole moment (e.g., Dickman and Clemens 1983); it thus becomes $N(\text{H}_2) = (4.0 \pm 2.0) \times 10^5 N(^{13}\text{CO})$. Excluding cloud 20, which is also a Lynds (1962) dark cloud, we have the necessary CO, ^{13}CO , and A_v data for only 10 lines of sight. The relationship between $N(\text{H}_{\text{total}})$ and $N(^{13}\text{CO})$ for these 10 low-extinction ($A_v < 1.6$ mag) lines of sight is $N(\text{H}_{\text{total}}) = (3.5 \pm 2.6) \times 10^6 N(^{13}\text{CO})$ with an intercept at $A_v = 0.0 \pm 0.7$ mag. The large uncertainties in the values are due to the small number statistics. $N(\text{H}_{\text{total}})$ is the quantity obtained from the extinction data because at the low extinctions prevalent in the high-

latitude-type clouds it cannot be assumed, as in Dickman (1978a), that all the hydrogen is molecular.

If it is assumed, as preliminary studies have indicated (MBM), that $N(\text{H I}) \sim N(\text{H}_2)$ in the high-latitude clouds, then $N(\text{H}_2) = (1.2 \pm 0.8) \times 10^6 N(^{13}\text{CO})$. Frerking, Langer, and Wilson (1982) obtain $N(\text{H}_2) = 6.7 \times 10^6 N(^{13}\text{CO})$ for extinctions $1 < A_v < 5$ mag in the Taurus clouds, but with variations of up to 1 order of magnitude. A similar study of the Perseus clouds by Bachiller and Cernicharo (1986) yields $N(\text{H}_2) = 3.8 \times 10^6 N(^{13}\text{CO})$.

In comparing the high-latitude clouds with the Dickman (1978a) sample, we are limited by the small number of lines of sight and by the uncertainty in the $N(\text{H I})/N(\text{H}_2)$ fraction. It is clear from the above results that the $N(\text{H}_2)/N(^{13}\text{CO})$ ratio in small molecular clouds varies by up to 1 order of magnitude. Since the previously obtained ratios range from 4.0×10^5 to 6.7×10^6 , the result obtained for the high-latitude molecular clouds is consistent with these determinations: the ^{13}CO abundances are similar to those found in dark clouds.

ii) W_{CO} and $N(\text{CO})$ Correlations

If W_{CO} and $N(\text{CO})$ are well correlated, the more easily obtainable quantity W_{CO} can be substituted for $N(\text{CO})$ as determined from LTE techniques to study the CO/ H_2 relationship. Using the CO and ^{13}CO data from Tables 3 and 4 and from Table 4 of MBM,⁵ but excluding the data for cloud 20 (which is excluded because it is a known dark cloud, L1642), $N(\text{CO})$ is obtained from the ^{13}CO data using LTE assumptions and a value for the CO/ ^{13}CO ratio. Penzias (1980)

⁵ The second entry for complex 22 in Table 4 of MBM should read $\delta = 69^\circ 38' 0$.

obtains a $\text{CO}/^{13}\text{CO}$ abundance ratio of 60 averaged for several Galactic lines of sight. Because the solar system $\text{C}/^{13}\text{C}$ value is 89, we choose a $\text{CO}/^{13}\text{CO}$ abundance of 75.

With $N(\text{CO})$ derived as described above, we can compare W_{CO} with $N(\text{CO})$ for the appropriate lines of sight. A least-squares-fit line to the 73 data points yields the following relationship: $W_{\text{CO}} = 2.1 \times 10^{-17} N(\text{CO}) + 3.37 \text{ K km s}^{-1}$, with a correlation coefficient of 0.41 and a better than 99.9% probability that the data are not taken from a random parent population. W_{CO} and $N(\text{CO})$, therefore, are well correlated in the core regions of the high-latitude molecular clouds. We can thus use W_{CO} to calibrate the CO/A_v and the $N(\text{CO})/N(\text{H}_2)$ ratios in the high-latitude clouds.

iii) W_{CO} and A_v Correlations

Given the good correlation between $N(\text{CO})$ as determined from LTE assumptions and W_{CO} , we now examine the relation between the two directly observable quantities: W_{CO} and A_B . The MWO CO data are chosen in order to minimize the problem resulting from the differing resolutions of the molecular and extinction data. Figure 3a shows all the available MWO W_{CO} data (266 lines of sight) plotted against the blue extinction. Although the data show considerable scatter, a trend toward greater W_{CO} with increasing A_B is noticeable. A least-squares fit to the data yields a linear relation with slope 1.1 ± 0.2 . The correlation coefficient, r , is 0.20, which, for the 266 lines of sight, gives a probability of better than 99.9% (Bevington 1969) that the data are not taken from an uncorrelated parent population.

We first assume that all the hydrogen along a line of sight is molecular; and then we will account for the H I contribution. Using the Bohlin, Savage, and Drake (1978) relation between $N(\text{H}_{\text{total}})$ and $E(B-V)$, a value of 3.1 for the ratio of visual extinction to color excess, and $A_v = 0.76 A_B$ (Dickman 1978b), the slope of the W_{CO} and A_v relation can be used to derive the ratio of the molecular hydrogen column density to the integrated $\text{CO}(J=1-0)$ antenna temperature $\{[N(\text{H}_2)/W_{\text{CO}}] \equiv X \text{ molecules cm}^{-2} \text{ K}^{-1} [\text{km s}^{-1}]^{-1}\}$. The slope of the MWO

data is thus equivalent to $X = (6.4 \pm 1.2 \times 10^{20} \text{ molecules cm}^{-2} \text{ K}^{-1} (\text{km s}^{-1})^{-1})$. The obtained value is ~ 2 times greater than the γ -ray value for GMCs (Bloemen *et al.* 1986) and is an upper limit to X because the contribution from H I has been ignored. Some determinations of the value of this parameter for other types of molecular cloud are tabulated by Bloemen *et al.* (1986).

In order to compare the high-latitude clouds with local dark clouds, the above analysis is applied to the data for the dark clouds presented by Dickman (1978a). The quantity W_{CO} is approximated by $T_A^* \Delta v$, and only the values of the red extinction which are not lower limits are chosen (the red extinction data were chosen because there are more red than blue data points) and converted to A_v in the standard manner (e.g., Dickman 1978b). The resulting least-squares fit for Dickman's sample of dark clouds yields $X = 4.7 \pm 1.1 \times 10^{20} \text{ molecules cm}^{-2} \text{ K}^{-1} (\text{km s}^{-1})^{-1}$. For these data, $r = 0.43$ and the probability that the data are not drawn from an uncorrelated sample is better than 99.9%. A similar analysis by Wouterloot (1981) on the Taurus clouds yields $X = 5.5 \times 10^{20} \text{ molecules cm}^{-2} \text{ K}^{-1} (\text{km s}^{-1})^{-1}$, with $r = 0.37$ and a better than 99.9% probability that the data are not drawn from an uncorrelated parent population. In all these cases, no account is taken of H I. These values for X are in reasonable agreement with those derived for the entire high-latitude cloud sample.

Clouds 18 and 20, which show a particularly strong correlation between W_{CO} and A_v , are also Lynds (1962) dark nebulae, with core visual extinctions of ≥ 2 mag. Since a strong correlation between W_{CO} and A_v is expected for these objects based on the study of Dickman (1978a), a least-squares fit is made for the high-latitude clouds excluding clouds 18 and 20 in order to determine if the strong correlation persists for the less obscured high-latitude clouds. The resulting linear relationship yields X of $(11.0 \pm 6.3) \times 10^{20} \text{ molecules cm}^{-2} \text{ K}^{-1} (\text{km s}^{-1})^{-1}$, with a correlation coefficient of 0.09 for the 203 lines of sight. This corresponds to a 20% probability that the data are taken from an uncorrelated parent population. The change in value and the now nonnegligible probability that the data are uncor-

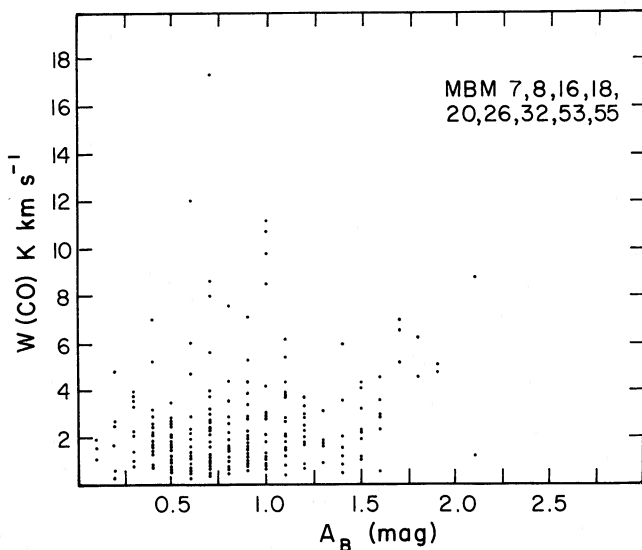


FIG. 3a

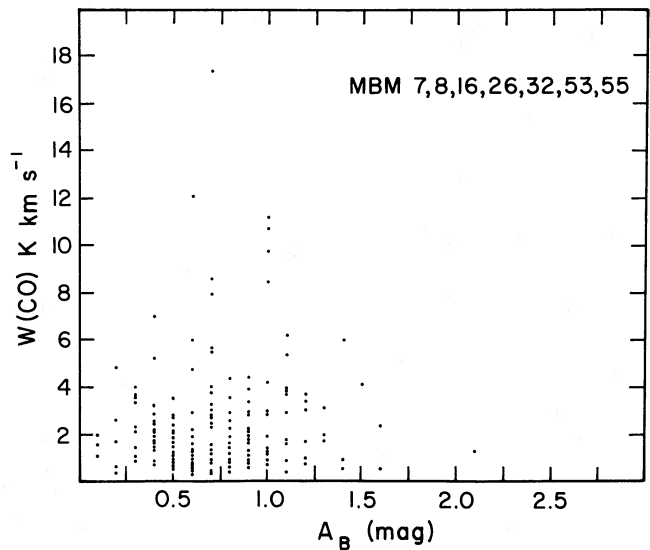


FIG. 3b

FIG. 3.—(a) The velocity-integrated $\text{CO}(J=1-0)$ antenna temperature (W_{CO}) vs. the blue extinction in magnitudes for all the high-latitude clouds with extinction and MWO CO data. (b) Same as (a) but not including clouds 18 and 20 which are also Lynds (1962) dark clouds.

related occur when less than 20% of the data are excluded. We therefore conclude that the good correlation between W_{CO} and A_v found for the data including clouds 18 and 20 is driven by the two dark molecular clouds. Figure 3b shows the plot for the 203 lines of sight excluding clouds 18 and 20.

Cloud 20 has a dark cloud core and a low extinction outer envelope and shows the breakdown of the W_{CO} to A_v relationship at the low extinctions. The 24 lines of sight in the cloud with $A_v \geq 1.1$ mag have a least-squares-fit line with a correlation coefficient of 0.83 which yields $X = 0.8 \times 10^{20}$ molecules $\text{cm}^{-2} \text{K}^{-1} (\text{km s}^{-1})^{-1}$, somewhat below the Dickman dark cloud value. The remaining 21 lines of sight with $A_v < 1.1$ mag show a correlation coefficient of -0.44 , indicative of either an anticorrelation or no correlation at all. This radical change in the W_{CO} to A_v relationship within the same cloud cannot be due to variations in the initial abundances, the external radiation field, or dust composition. The breakdown of the relationship appears to indicate a change in the physical conditions at low extinctions, in the high-latitude clouds and in the envelopes of dark clouds.

Because the correlation is much weaker when clouds 18 and 20 are excluded from the sample, the slope of the least-squares-fit line is not a meaningful way of determining X from the remaining sample; the weighted average for the data points is probably more meaningful. The weighted average for the 203 points yields an X value of 3.2×10^{20} molecules $\text{cm}^{-2} \text{K}^{-1} (\text{km s}^{-1})^{-1}$, with an uncertainty in the mean of 0.1×10^{20} and with individual clouds showing X values from 1.0×10^{20} to 6.1×10^{20} molecules $\text{cm}^{-2} \text{K}^{-1} (\text{km s}^{-1})^{-1}$, with mean uncertainties ranging from 0.2 to 0.6×10^{20} . The measurement errors are much smaller than the cloud-to-cloud variations in the X value. We therefore conclude that the variations in X from cloud to cloud are real, and attempts to use a global value of X in determining masses and molecular column densities for small molecular clouds will result in errors of factors of a few.

The above analysis has not included the contribution to the extinction from the H I associated with the cloud. The only fully sampled H I observations to date on the high-latitude clouds are at a resolution of $21'$ (Magnani 1987) and thus do not shed light on the behavior of the H I component at the angular resolution of the extinction or of the CO data. Nevertheless, a lower limit to the value of X may be obtained by overestimating the H I contribution to the $N(\text{H}_{\text{total}})-A_v$ relationship for the high-latitude clouds. Such a procedure is detailed in Magnani (1987). The resulting lower limit to X , $\sim 1 \times 10^{20}$ molecules $\text{cm}^{-2} \text{K}^{-1} (\text{km s}^{-1})^{-1}$, is a lower limit consistent with the previous determination based on the weighted average and with determinations of X for other molecular clouds (Bloemen *et al.* 1986).

Recently, de Vries, Heithausen, and Thaddeus (1987) have determined X for the molecular complex which includes clouds 26 to 32. $N(\text{H}_2)$ is determined from the $100 \mu\text{m}$ IRAS data after background removal and calibration for the H I contribution. The resulting value of X , $0.5 \pm 0.3 \times 10^{20}$ molecules $\text{cm}^{-2} \text{K}^{-1} (\text{km s}^{-1})^{-1}$, is significantly lower than what we obtain for the high-latitude clouds in general and for the two clouds in our sample which overlap the de Vries, Heithausen, and Thaddeus study (cloud 26 has $X = 4.8 \pm 0.6 \times 10^{20}$ and cloud 32 has $X = 2.6 \pm 0.4 \times 10^{20}$ molecules $\text{cm}^{-2} \text{K}^{-1} [\text{km s}^{-1}]^{-1}$). Our values for X are determined from the weighted average of the individual points while de Vries, Heithausen, and Thaddeus (1987) use a best-fit line through their data to determine X . Although the reason for these differences is not fully clear,

we point out the following: because the average W_{CO} over their examined region is 1 K km s^{-1} , $X = 0.5 \times 10^{20}$ molecules $\text{cm}^{-2} \text{K}^{-1} (\text{km s}^{-1})^{-1}$, and the Bohlin, Savage, and Drake (1978) relation should be valid for these objects, the expected visual extinction averaged over the molecular clouds due to molecular hydrogen is ~ 0.06 mag. Magnani and de Vries (1986) obtain from star counts a visual extinction relative to the background of 0.7 mag for cloud 26 and 0.3 mag for cloud 32. Since the H I and H₂ content of the high-latitude clouds appears to be roughly equal (see MBM), it seems unlikely that the molecular content of the de Vries, Heithausen, and Thaddeus (1987) clouds should contribute so little to the overall extinction. Star counts to determine the extinction over a significant portion of the area studied by de Vries, Heithausen, and Thaddeus should clarify this situation.

We now consider the sources of uncertainty in the above analysis. The resolution of the star counts is $8'$, substantially coarser than the MWO CO($J=1-0$) resolution ($\sim 2.3'$). As discussed above, clumping in CO emission at size scales of a few arcminutes may introduce some small errors in the analysis, but these will not affect the basic conclusions of this paper.

The small number of stars in an $8'$ pixel at high latitudes produces a large uncertainty in the determination of the extinction. Since the relative uncertainty in the extinction ($\Delta A_v/A_v$) in an $8'$ pixel is ~ 0.7 and the relative uncertainty in W_{CO} is only 0.15, the uncertainty in any individual measurement of X is dominated by the uncertainty in A_v .

The dispersion of the data points, excluding clouds 18 and 20, from the least-squares-fit line is nearly twice the dispersion expected from the combination of the uncertainties in A_v and W_{CO} . At the low extinctions typical of the clouds in the sample ($A_v \lesssim 1$ mag) only 25% of the uncertainty is due to measurement error. Therefore, the large deviations from the best-fit line are real and are not due to uncertainties in the measured quantities. The 266 data points in the complete sample imply a relative uncertainty in X of ~ 0.05 for the sample mean, and $\sim 0.08-0.23$ for individual objects. Thus, the variation in X from object to object is greater than what can be accounted for from uncertainties in the extinction or W_{CO} .

The reasons for the breakdown of the W_{CO} to A_v correlation at low extinction are not clear as of this writing. Some of the possibilities include the following:

1. W_{CO} [and thus $N(\text{CO})$; see § IVa(ii)] is not a good tracer of $N(\text{H}_2)$ for $A_v \lesssim 1$ mag.
2. W_{CO} traces $N(\text{H}_2)$ well even at $A_v \lesssim 1$ mag, but the non-negligible contribution of $N(\text{H I})$ at these low extinctions destroys the good correlation between W_{CO} and A_v (because the latter quantity traces H_{total} and not solely H_2).
3. The CO/A_v ratio is not constant for $A_v \lesssim 1$ mag.
4. The young age of the high-latitude clouds ($< 10^6$ yr; MBM) may mean that the chemistry of these objects has not had time to produce equilibrium abundances ($\sim 3 \times 10^6$ yr; e.g., Williams 1985). Specifically, the conversion of H to H₂ has not had time to be completed.
5. Changes in the UV radiation field from object to object may produce large variations in the photodissociation rate which will, in turn, affect the CO/A_v ratio. This point is discussed in greater detail in § IVb(iv).

The results from §§ IVa(i)-IVa(iii) are summarized in Table 5. From this table we may conclude the following:

1. $N(\text{H}_2)/N(^{13}\text{CO})$ for the high-latitude clouds is consistent with the range of values derived by Dickman (1978a), Frerking,

Langer, and Wilson (1982), and Bachiller and Cernicharo (1986) for various dark clouds.

2. Although there is considerable scatter in the value of $N(\text{H}_2)/W_{\text{CO}}$ for the high-latitude clouds depending on the sample and assumptions about $N(\text{H I})$, the values are reasonably close to the value obtained for dark clouds from the sample of Dickman (1978a).

3. There is no best value for $N(\text{H}_2)/W_{\text{CO}}$ in the high-latitude clouds. The value depends on whether one considers the dark cloud high-latitude clouds, the dark cores of the high-latitude clouds, the low-extinction high-latitude clouds and envelopes, and the contribution of H I to H_{total} .

4. Only the high-extinction regions ($A_v \gtrsim 1$ mag) show a good $N(\text{H}_2)/W_{\text{CO}}$ correlation.

5. The values obtained for $N(\text{H}_2)/W_{\text{CO}}$ are typically a factor of 5 higher than the value obtained by de Vries, Heithausen, and Thaddeus (1987) for the region they analyzed.

b) Abundances

i) CO Column Densities and Abundances

The value of $N(\text{CO})$ is derived from the CO and ^{13}CO data using an LTE analysis. The quantity T_R is determined from the CO data as described in § IIc. With T_R , the $\text{CO}(J=1-0)$ excitation temperature is obtained, and is used along with $T_R(^{13}\text{CO})$, $\Delta v(^{13}\text{CO})$, and LTE assumptions (see Dickman 1978a) to determine the column density of ^{13}CO for the particular line of sight. Dickman (1978a) and Kutner and Leung (1985) discuss the validity of this method. For the density and temperature regime relevant to the high-latitude molecular clouds it is unlikely that the LTE method yields $N(^{13}\text{CO})$ with an uncertainty of more than a factor of 2 or 3.

The ^{13}CO data currently are available only for the core regions of high-latitude molecular clouds. Although the values of $N(\text{CO})$ and the $N(\text{CO})/N(\text{H}_2)$ ratio obtained in this manner are relevant only for the densest and most obscured areas of the high-latitude molecular clouds, the extinction in those regions is still lower than the extinction in the cores of dark molecular clouds. For the 30 lines of sight where we observed ^{13}CO at MWO, the average $N(\text{CO})$ value is $6.1 \pm 1.3 \times 10^{16} \text{ cm}^{-2}$; for the 41 lines of sight where the 12 m data are available, the average $N(\text{CO})$ value is $6.4 \pm 0.6 \times 10^{16} \text{ cm}^{-2}$.

The abundance of CO expressed as the $N(\text{CO})/N(\text{H}_2)$ ratio can be obtained using the above values for $N(\text{CO})$ and values for $N(\text{H}_2)$ obtained from the extinction. In the following analysis, we ignore the contribution of H I which is not a good assumption for the high-latitude clouds. However, the $N(\text{CO})/N(\text{H}_2)$ abundance will be underestimated by no more than a factor of a few (based on H I observations) and thus will not affect the conclusions of this section. There are only 10 lines of sight where CO, ^{13}CO , and A_v data are all available. These 10 lines of sight produce an $N(\text{CO})/N(\text{H}_2)$ ratio of $1.2 \pm 0.6 \times 10^{-4}$.

The $N(\text{CO})/N(\text{H}_2)$ ratio can also be obtained by approximating $N(\text{H}_2)$ using the value of X determined in the previous section ($3.2 \times 10^{20} \text{ molecules cm}^{-2} \text{ K}^{-1} [\text{km s}^{-1}]^{-1}$) and the value of W_{CO} for the given line of sight. Of course, this technique does not provide independent determinations of $N(\text{H}_2)$ and $N(\text{CO})$, but within the uncertainty in X , the value of $N(\text{CO})/N(\text{H}_2)$ should be as reliable as that determined with $N(\text{H}_2)$ calculated from the extinction data.

Using the value of X determined in the previous section gives a value for the $N(\text{CO})/N(\text{H}_2)$ ratio of $4.6 \pm 0.5 \times 10^{-5}$ for the 30 lines of sight for which both W_{CO} and extinction are

available. Using the 12 m data, an $N(\text{CO})/N(\text{H}_2)$ ratio of $4.4 \pm 0.4 \times 10^{-5}$ is obtained for the 41 lines of sight in Table 4. The value of $N(\text{CO})/N(\text{H}_2)$ in the core regions of the high-latitude molecular clouds is thus $\sim (4-12) \times 10^{-5}$. We therefore conclude that the mean CO abundance in the high-latitude clouds is not significantly different from that found in dark clouds.

ii) OH Column Densities and Abundances

$N(\text{OH})$ is obtained from the data in Table 1 by using the following equations:

$$T_{A,i} = \eta_B F (T_{\text{ex},i} - T_{\text{BG}}) (1 - e^{-\tau_i}) \text{ K}, \quad (1)$$

and

$$N(\text{OH}) = C_i T_{\text{ex},i} \Delta v_i \tau_i \text{ cm}^{-2}. \quad (2)$$

$T_{A,i}$ is the antenna temperature of the i th transition, η_B is the beam efficiency (~ 0.8 for the Green Bank 43 m telescope at these frequencies; Ron Maddalena, personal communication), F is the source filling factor, $T_{\text{ex},i}$ and τ_i are the excitation temperature and optical depth of the i th transition (Wouterloot 1981), respectively, T_{BG} is the background temperature, $N(\text{OH})$ is the column density in cm^{-2} , C_i is a constant equal to $4.30 \times 10^{14} \text{ cm}^2 \text{ K}^{-1} (\text{km s}^{-1})^{-1}$ for the 1665 MHz transition and $2.39 \times 10^{14} \text{ cm}^2 \text{ K}^{-1} (\text{km s}^{-1})^{-1}$ for the 1667 MHz transition, and Δv_i is the line FWHM in km s^{-1} .

$T_{\text{ex}}(1665)$ is set equal to $T_{\text{ex}}(1667)$ in order to reduce the number of unknowns and allow a solution to the two pairs of equations. This assumption is valid in the presence of normal excitation (see the Appendix). Assuming that $T_{\text{BG}} = 3.2 \text{ K}$ (Wouterloot 1981) and that the filling factor of OH in the telescope beam is unity, the optical depths and column densities for the transitions are obtained.

If the ratio of the 1667/1665 antenna temperatures or the 1667/1665 integrated antenna temperatures are ~ 1.0 , the transitions are probably optically thick. Two lines of sight (clouds 21 and 38) showed optically thick emission, and the above equations could not be solved for one line of sight (cloud 26) so that $N(\text{OH})$ was not obtained for these cases.

The column densities for the 15 lines of sight range from 2.0×10^{13} to $3.7 \times 10^{15} \text{ cm}^{-2}$ with a mean of $9 \times 10^{14} \text{ cm}^{-2}$. The values for the observed lines of sight are shown in column (6) of Table 6. The values of $N(\text{OH})$ are, of course, averaged over the OH beam (18'). The presence of clumps several arcminutes in size (Magnani 1987) may lead to greater column density estimates. Observations at higher resolutions are needed to resolve this issue.

To calculate the abundance of OH with respect to H_{total} we use $N(\text{H}_{\text{total}})$ as determined from the extinction. $N(\text{OH})/N(\text{H}_{\text{total}})$ for the eight lines of sight shows a mean value of 2×10^{-6} and a range from 2×10^{-7} to 4×10^{-6} ; the values are presented in column (8) of Table 6.

Table 7 lists the range and mean value of $N(\text{OH})$ and the $N(\text{OH})/N(\text{H}_{\text{total}})$ ratio for dark dust clouds, diffuse clouds, and the high-latitude clouds. As is clear from the table, there is no typical value for $N(\text{OH})$ in dark clouds; values range from 10^{13} to 10^{15} cm^{-2} and the mean values by various authors show a clustering around 10^{14} – 10^{15} cm^{-2} . For the diffuse molecular clouds, however, $N(\text{OH})$ is of order 10^{13} cm^{-2} , with no value greater than $1 \times 10^{14} \text{ cm}^{-2}$, significantly lower than is found in the dark clouds. The high-latitude clouds thus show OH abundances and column densities greater than those in the diffuse molecular clouds.

TABLE 6
OH MAIN-LINE RATIOS, COLUMN DENSITIES, AND ABUNDANCES

| Cloud | R | 1 σ | R' | 1 σ | $N(\text{OH})$ (cm^{-2}) | A_v (mag) | $N(\text{OH})/N(\text{H}_2)$ |
|---------|-----|------------|-----|------------|--|------------------|------------------------------|
| 6..... | 1.7 | 0.30 | 1.8 | 0.51 | 6.8×10^{13} | ... | ... |
| 7..... | 1.9 | 0.63 | 1.3 | 0.77 | 1.1×10^{15} | 0.8 | 1.5×10^{-6} |
| 16..... | 1.4 | 0.35 | 1.2 | 1.01 | 3.0×10^{15} | 0.8 | 4.0×10^{-6} |
| | 1.5 | 0.28 | 1.9 | 0.59 | 1.6×10^{14} | 0.8 | 2.0×10^{-7} |
| 20..... | 1.4 | 0.25 | 2.0 | 0.56 | 1.8×10^{14} | 1.1 | 1.6×10^{-7} |
| 21..... | 0.8 | 0.13 | 1.0 | 0.23 | 6.2×10^{13} | ... | ... |
| 26..... | 1.1 | 0.39 | 2.5 | 1.44 | ... ^a | 0.7 | ... |
| 28..... | 1.9 | 0.51 | 1.4 | 0.52 | 3.7×10^{15} | ... | ... |
| 30..... | 1.5 | 0.22 | 1.3 | 0.35 | 8.6×10^{14} | ... | ... |
| 32..... | 2.1 | 0.65 | 1.5 | 0.87 | 5.9×10^{14} | 0.4 | 1.6×10^{-6} |
| 38..... | 0.9 | 0.37 | 1.4 | 0.82 | 3.6×10^{13} | ... | ... |
| 40..... | 2.3 | 0.57 | 2.9 | 1.05 | 5.5×10^{13} | ... | ... |
| | 2.0 | 0.54 | 1.4 | 0.67 | 5.5×10^{14} | ... | ... |
| 55..... | 1.7 | 0.41 | 1.8 | 0.69 | 1.8×10^{14} | 0.4 | 4.8×10^{-7} |
| | 1.5 | 0.83 | 8.1 | 7.58 | 4.0×10^{13} | 0.6 ^b | 3.8×10^{-6} |
| | 2.2 | 0.44 | 1.2 | 0.61 | 2.2×10^{15} | | |
| | 1.4 | 0.82 | 4.2 | 3.83 | 2.0×10^{13} | | |

^a No solution.

^b Three components along line of sight.

The $N(\text{OH})/A_v$ ratios in the high-latitude clouds and the dark clouds indicate that two populations of clouds may exist; one with an $N(\text{OH})/A_v$ ratio $\sim 10^{14} \text{ cm}^{-2} \text{ mag}^{-1}$ and one with an $N(\text{OH})/A_v$ ratio $\sim 10^{15} \text{ cm}^{-2} \text{ mag}^{-1}$. A survey of some of the literature cited in Table 7 by Crutcher (1979) led him to conclude that the $N(\text{OH})/A_v$ ratio exhibits a constant value of $8 \times 10^{13} \text{ cm}^{-2} \text{ mag}^{-1}$, with the exceptions of W44 and the Taurus region which have $N(\text{OH}) \sim 10^{15} \text{ cm}^{-2}$ independent of extinction. Crutcher (1979) explains these discrepant results as

due to anomalous excitation conditions which have led the previous researchers to overestimate $N(\text{OH})$ in the Taurus region. In the Appendix, we show that our results are little affected by anomalous excitation effects and that it is unlikely that we have overestimated $N(\text{OH})$ along the lines of sight to the high-latitude clouds.

iii) H_2CO Column Densities and Abundances

The H_2CO column density is obtained following Cohen *et al.* (1983) from the equation

$$N(\text{H}_2\text{CO})_i = 1.45 \times 10^{13} T_{\text{ex}} \int -T_B dv \text{ cm}^{-2}, \quad (3)$$

where $N(\text{H}_2\text{CO})_i$ represents the column density of H_2CO in the 1_{11} state, T_{ex} is the excitation temperature (which we assume to be 1.7 K following Cohen *et al.* 1983), T_B is the brightness temperature at the telescope, and v is the radial velocity in km s^{-1} . For the 49 lines of sight with H_2CO detections (including the lines of sight in the two mapped regions), $N(\text{H}_2\text{CO})$ ranges from 1.2×10^{12} to $9.8 \times 10^{12} \text{ cm}^{-2}$, with a mean of $4.6 \pm 0.3 \times 10^{12} \text{ cm}^{-2}$.

A plot of the H_2CO brightness temperature against the visual extinction shows considerable scatter with a least-squares-fit line having a slope of 0.13 ± 0.07 . This result is comparable to the results found by several authors for regions in dark clouds with visual extinction greater than 2 mag (Turner and Heiles 1974; Sherwood and Wilson 1981; Pöppel, Rohlfs, and Celnik 1983; and Toriseva and Mattila 1985). However, the correlation coefficient for the high-latitude cloud data is -0.17 . This very poor or nonexistent correlation is in contrast to what is found in the H_2CO dark cloud studies, where the correlation coefficients range from 0.39 to 0.77.

Along the 16 lines of sight where we have both H_2CO detections and CO data, we note that $N(\text{H}_2\text{CO})$ and W_{CO} are well

TABLE 7
OH IN DARK CLOUDS AND DIFFUSE CLOUDS

| Cloud | Range ($\times 10^{13} \text{ cm}^{-2}$) | Mean ($\times 10^{13} \text{ cm}^{-2}$) | $N(\text{OH})/N(\text{H})$ | Number of Lines of Sight | References |
|----------------------------|---|--|----------------------------|-----------------------------|------------|
| Dark dust clouds | 1.7-19 | 6.4 | ... | 10 | 1 |
| | 0.3-21.7 | 5.7 | ... | 5 | 2 |
| | 77-594 | 335 | ... | 3 | 3 |
| | 9.3-160 | 55 | ... | 9 | 4 |
| | 0.2-200 | ~ 10 | ... | ~ 50 | 5 |
| | 50-580 | 178 | ... | 17 | 6 |
| | 60-400 | ~ 110 | ... | 22 | 7 |
| | ... | 71 ^a | ... | 20 | 8 |
| | ... | 150 ^b | ... | ... | ... |
| | ... | ~ 10 | 2×10^{-7} | 68 | 9 |
| | ... | ~ 30 | 4×10^{-8} | 4 | 10 |
| | 8-70 | ... | 2.7×10^{-8c} | 38 | 11 |
| | ... | ... | 2×10^{-7} | ... | 12 |
| Diffuse Clouds | 5.1-9.7 | 7.4 | ... | 2 | 13 |
| | ... | 5.2 | ... | 1 | 14 |
| | 0.4-6.3 | 3.9 | 1.0×10^{-7} | 9 | 15 |
| | ... | 9 ^a | 1.3×10^{-7a} | 6 | 16 |
| High-Latitude Clouds | 2.0-370 | 91 | 2×10^{-6c} | 13 | 17 |

^a Assuming $T_x(\text{OH}) = 5 \text{ K}$.

^b Assuming $T_x(\text{OH}) = 8 \text{ K}$.

^c $N(\text{OH})/N(\text{H}_2)$.

REFERENCES.—(1) Heiles 1968; (2) Heiles 1969; (3) Turner and Heiles 1971; (4) Knapp and Kerr 1973; (5) Myers 1973; (6) Turner 1973; (7) Turner and Heiles 1974; (8) Myers 1975; (9) Sancisi *et al.* 1974; (10) Crutcher 1977, 1979; (11) Myers *et al.* 1978; (12) Wouterloot 1981; (13) Crutcher and Watson 1976; (14) Chaffee and Lutz 1977; (15) Nguyen-Q-Rieu *et al.* 1976; (16) Kazés, Crovisier, and Aubry 1977; (17) This paper.

correlated. This correlation is seen by comparing Figures 2a and 2c, the velocity-integrated H_2CO brightness temperature (W_{H_2CO}) and W_{CO} , respectively, for one of the core regions of cloud 55. By examining equation (3), it is evident that $N(H_2CO)$ is just W_{H_2CO} times a constant. The correlation coefficient for the 16 $N(H_2CO)$ and W_{CO} data points is 0.75 with a probability $> 99.9\%$ that the sample is correlated. This correlation is noteworthy in view of the fact that both CO and H_2CO are individually poorly correlated with A_v in the more transparent high-latitude clouds.

Although we detect H_2CO absorption from lines of sight where the extinction is lower than is usually required for the detection of the 6 cm H_2CO line, there are many other lines of sight in the high-latitude clouds at comparable or higher extinctions which show no traces of H_2CO . This phenomenon is also noticed in clouds with substantially higher extinctions. Figure 4 of Myers *et al.* (1978) shows many high-extinction lines of sight in the ρ Oph cloud where 6 cm H_2CO absorption is not detected. The presence of H_2CO at low extinctions is therefore not well correlated with the extinction and must depend on some other quantity.

The slope of the least-squares-fit line to the above data gives a value of $N(H_2CO)/W_{CO} = 1.1 \pm 0.3 \times 10^{12}$ molecules $cm^{-2} K^{-1} (km s^{-1})^{-1}$ corresponding to an abundance relation $N(H_2CO)/N(CO)$ of $\sim 2.3 \times 10^{-5}$ based on the $W_{CO}/N(CO)$ ratio from § IVa(ii). The $N(H_2CO)/W_{CO}$ ratio, when divided by the X value determined in § IVa(iii), gives the abundance of the H_2CO with respect to H_2 . The $N(H_2CO)/N(H_2)$ ratio determined in this fashion is 3.4×10^{-9} , within a factor of 6 of the value in dark clouds determined by Batrla, Walmsley, and Wilson 1984, within a factor of 3 of the value derived for three dark clouds (Sume, Downes, and Wilson 1975; Evans and Kutner 1976; Downes, Wilson, and Bieging 1976), and virtually identical to the value obtained by Kutner (1973) for the Taurus dark clouds.

The $N(H_2CO)/N(H_{total})$ ratio is also obtained with $N(H_{total})$ determined from the extinction data. Because of the lack of correlation between $T_B(H_2CO)$ and A_v , we determine the H_2CO abundance from the mean of the $N(H_2CO)/N(H_{total})$ values (rather than from the best-fit line). For 16 lines of sight we obtain $N(H_2CO)/N(H_{total}) = 1.9 \pm 0.4 \times 10^{-9}$.

The abundance of H_2CO in the high-latitude clouds is in the same range as the dark cloud abundance which ranges from 2×10^{-9} to 2×10^{-8} . In diffuse clouds, H_2CO is not detected at all, and gas phase chemistry models (e.g., Viala 1986) predict H_2CO abundances less than 10^{-12} . As in the case of CO and OH, the H_2CO abundance in the high-latitude molecular clouds more closely resembles the dark cloud abundance. Although the extinctions in the high-latitude clouds are more similar to the diffuse molecular cloud extinctions, the gas phase chemistry seems to produce dark cloud abundances.

iv) CO Self-Shielding

The $N(CO)/N(H_2)$ ratio varies dramatically between dark and diffuse molecular clouds. In dark clouds its value is $\sim (5-10) \times 10^{-5}$ (Dickman 1975; Young *et al.* 1982), while in diffuse clouds it is not constant and is generally 2 orders of magnitude smaller than the dark cloud value (Federman *et al.* 1980; Williams 1985; van Dishoeck and Black 1987; Lada and Blitz 1987). Even within an individual cloud, the $N(CO)/N(H_2)$ ratio may vary by 3 orders of magnitude from the core to the transparent edge (Young *et al.* 1982).

The core regions of high-latitude clouds show an

$N(CO)/N(H_2)$ ratio similar to that found by Dickman (1978a) for the cores of dark clouds, although the visual extinctions in his sample range from 1.5 to 10 mag, while the extinction in the core regions of high-latitude molecular clouds is significantly lower, ranging from 0.45 to 2.1 mag (Magnani and de Vries 1986). This phenomenon has been noticed previously for a few molecular clouds (e.g., Crutcher 1980). Although the exact value of the $N(CO)/N(H_2)$ ratio in the cores of the high-latitude clouds may vary by a factor of 2 or 3, it is clear that the ratio obtained in § IVb(i) ($[4-12] \times 10^{-5}$) is at least 1–2 orders of magnitude greater than the abundance ratio obtained from UV observations of diffuse clouds with visual extinctions < 0.5 mag and 2–3 orders of magnitude greater than the abundance ratio Young *et al.* (1982) determine for the outer edge of B5 where $A_v < 2$ mag.

The enhanced CO column density in the low-extinction high-latitude clouds compared to diffuse molecular clouds, may be understood in light of recent work on the shielding of CO from dissociating radiation (Glassgold, Huggins, and Langer 1985, hereafter GHL; van Dishoeck and Black 1987).

In the GHL model, the photodissociation of CO results from line, rather than from continuum, radiation, so that the CO shields itself with additional shielding provided by H_2 and dust. For a model cloud temperature of 20 K and $n(H_2)$ of $10^3 cm^{-3}$, conditions which are reasonable for the higher density clumps of the high-latitude molecular clouds (Magnani 1987), GHL derive an $N(CO)/N(H_2)$ ratio of $\sim 5 \times 10^{-5}$ and $N(CO) > 10^{16} cm^{-2}$ for visual extinctions as low as 0.8 mag.

The model of van Dishoeck and Black (1987) treats the “translucent” ($1 mag < A_v < 5 mag$) photochemical zone in molecular clouds in detail, incorporating the most recent laboratory data on photodissociation. Model 3 of van Dishoeck and Black (1987) reproduces the CO abundance we derive for high-latitude clouds with visual extinctions of 0.6 and 1.0 mag if the ultraviolet radiation field the clouds are exposed to is smaller than that the average interstellar UV field proposed by Draine (1978) by a factor of 2.5 and 1.7, respectively. Such fluctuations in the interstellar UV field are plausible because of the asymmetrical UV illumination provided by early-type stars in the Galactic plane. Similarly, Crutcher (1980) attributes the high CO/A_v ratio in the diffuse cloud toward 3C 123 as perhaps due to the much reduced radiation field to which the cloud is exposed.

The two models thus reproduce the CO column densities and abundances of the high-latitude molecular clouds provided certain parameters (such as radiation field, temperature, etc.) are varied and/or the density of the CO clumps within the telescope beam is of order $10^3 cm^{-3}$.

v) Are the Enhanced Abundances Produced by Shocks?

The OH and H_2CO abundances and column densities in the high-latitude molecular clouds cannot be reproduced by the most recent chemical equilibrium diffuse cloud models. Viala (1986) has developed a steady state model of interstellar diffuse and dark clouds which includes the absorption of UV photons by dust grains and by the gas and an improved treatment of the UV photodissociation process over previous models. For a model “moderately diffuse” cloud with $A_v = 1$ mag, $N_H = 2 \times 10^{21}$, $T = 50$ K, and $n = 100, 500,$ and $1000 cm^{-3}$, the OH and H_2CO abundances are $9.4 \times 10^{-9}, 4.4 \times 10^{-9}, 3.8 \times 10^{-9}$ and $3.7 \times 10^{-14}, 3.3 \times 10^{-13}, 9.3 \times 10^{-13}$, respectively. These values are several orders of magnitude less than what we have found for the high-latitude clouds.

Van Dishoeck and Black (1986) employ a model which features a corrected description of radiative transfer in the H_2 lines and continuous gradients of temperature and density across the model diffuse clouds. The values of $N(OH)$ for several model clouds are of order 10^{13} cm^{-2} , 1–2 orders of magnitude less than what we determine for the lines of sight to the core regions of the high-latitude clouds. $N(H_2CO)$ is not included in their model because current diffuse cloud chemistry schemes do not predict significant quantities of this molecule.

A possible way to achieve the high observed abundances of OH and H_2CO is through the compression and heating of the ambient medium by nondissociative shocks. Mitchell and Deveau (1983) calculate the abundance profiles of various molecules as a function of time and give values of the postshock column densities after the passage of a 10 km s^{-1} shock through a diffuse interstellar cloud of initial density 100 cm^{-3} . After a few times 10^3 yr , OH abundances of order 10^{-6} and H_2CO abundances of order 10^{-8} are predicted. The column density of OH increases from $1.4 \times 10^{12} \text{ cm}^{-2}$ to $4.4 \times 10^{14} \text{ cm}^{-2}$, while $N(H_2CO)$ increases from 3.3×10^7 to $9.5 \times 10^{12} \text{ cm}^{-2}$. Although the initial density of the cloud used in the Mitchell and Deveau (1983) model is probably greater than what is expected in the normal ISM, the concept that the production of high molecular abundances occurs in nondissociative shocks is supported by the presence of many high-latitude clouds within the rims of Heiles (1984) H I supershells (Blitz 1987).

If shocks are to explain the observed OH and H_2CO abundances in the high-latitude clouds, one would then expect the enhancement of other molecular species (such as CH^+ or HCO^+) over their diffuse cloud values. Observations of other shock-produced species should provide strong confirmation or refutation of the shock formation hypothesis.

In addition, the formation of the high-latitude clouds in shocks would explain two of the more puzzling aspects of the high-latitude clouds: the complicated velocity structure of these objects and the many gravitationally unbound clouds (MBM), and also, perhaps, the presence of unusual wings in some of the CO emission profiles (Blitz, Magnani, and Wandel 1987).

V. SUMMARY

This paper discusses the CO, OH, and H_2CO abundances and column densities of the high-latitude molecular clouds. Some of the properties of these objects resemble those of dark molecular clouds (size, mass, CO, OH, and H_2CO line profiles), while the extinction resembles that of diffuse molecular clouds. Since the extinction is one of the key factors in determining the gas phase chemistry in molecular clouds, and since the abundances of various molecules differ significantly in the two types of molecular clouds, an investigation into the abundances of the high-latitude molecular clouds was initiated. The results presented in this paper establish that the high-latitude molecular clouds in the observed sample have abundances and column densities more similar to those found in dark clouds than to the abundances in the diffuse molecular clouds.

The CO abundance with respect to H_2 is comparable to what is found for dark clouds ($[5-10] \times 10^{-5}$). Although the CO column densities are typically of order 10^{16} cm^{-2} , down by 1 order of magnitude from the dark cloud value, the abundance of CO with respect to H_2 is similar to that in dark clouds because $N(H_2)$ is also lower by a factor of 10 in the high-latitude molecular clouds. Both the abundance and the column

density of CO are orders of magnitude greater than what is determined from UV observations of diffuse molecular clouds.

In the case of H_2CO , the derived abundance is within factors of a few of the values found in dark cloud surveys. The column densities of H_2CO in the high-latitude clouds are lower by about 1 order of magnitude with respect to dark clouds, but $N(H_2CO)$ in the high-latitude clouds is many orders of magnitude greater than what is expected for diffuse clouds where H_2CO has never been detected.

The OH abundance in the high-latitude clouds is an order of magnitude greater than the value determined for dark clouds (10^{-6} as opposed to 10^{-7}). This leads to OH column densities which are comparable to those in dark molecular clouds (10^{14} – 10^{15} cm^{-2}). Although the OH abundance in diffuse clouds is similar to the dark cloud value, $N(OH)$ for diffuse clouds is of order 10^{13} cm^{-2} , 1 order of magnitude less than the high-latitude cloud value.

The analysis of the data from the three observed molecular species indicates that the high-latitude clouds show abundances and column densities more similar to those of the dark clouds than to those of the diffuse clouds. There are differences between the high-latitude clouds and the dark clouds, however. For the high-latitude clouds, neither W_{CO} nor W_{H_2CO} correlate as well with extinction as they do in dark clouds. Surprisingly, W_{CO} and W_{H_2CO} do correlate well with each other.

The breakdown in the W_{CO} and A_v correlation occurs at $A_v \lesssim 1 \text{ mag}$ for the high-latitude molecular clouds in general and at $A_v \lesssim 1.1 \text{ mag}$ for cloud 20 in particular. The uncertainties in A_v and W_{CO} are not sufficient to explain the scatter in the W_{CO} to A_v relation for the high-latitude molecular clouds. Because at these low extinctions W_{CO} correlates well with $N(CO)$ and A_v correlates well with $N(H_2)$, the scatter in the W_{CO} to A_v relation implies that there should exist scatter in the $N(CO)/N(H_2)$ ratio for clouds with $A_v \lesssim 1 \text{ mag}$.

In spite of the scatter in the W_{CO} to A_v relation, the weighted average value of X ($3.2 \times 10^{20} \text{ molecules cm}^{-2} \text{ K}^{-1} [\text{km s}^{-1}]^{-1}$) is calculated and found to be approximately the same for high-latitude clouds and both dark clouds and GMCs. However, the high-latitude clouds show a real variation in X from cloud to cloud ($[1-6] \times 10^{20} \text{ molecules cm}^{-2} \text{ K}^{-1} [\text{km s}^{-1}]^{-1}$) rendering $N(H_2)$ determinations by the $N(H_2)/W_{CO}$ ratio uncertain by nearly 1 order of magnitude. Indiscriminate application of a single X value to different low-extinction molecular clouds will lead to errors in $N(H_2)$ and mass determinations.

Extant diffuse gas chemistry and photodissociation models are able to reproduce the CO column densities in the high-latitude clouds if the radiation field the clouds are exposed to is less intense by factors of a few than the normal interstellar radiation field and/or if the clouds have clumps with density $\sim 10^3 \text{ cm}^{-3}$. The existing models, however, cannot produce OH and H_2CO in the low-extinction clouds in sufficient quantities. A promising method of producing the enhanced abundances of OH and H_2CO may be through nondissociative shocks. The creation of high-latitude type clouds in such shocks may also explain the complex velocity structure in these objects, the peculiar wings observed along certain lines of sight, and the tendency for many of the high-latitude clouds to lie along the rims of H I supershells. Observations of species which are specifically enhanced in shocks such as CH^+ or HCO^+ may settle this issue and elucidate the relationship of high-latitude molecular clouds to the other types of small molecular cloud.

We would like to thank Lee Armus, Susan Hoban, and Jerome Barkum for help with the OH observations and Mike Hauser, Steve Federman, Frank Kerr, Don Wentzel, and J.-P. Caillault for insightful comments on the manuscript. We gratefully acknowledge partial support from grant AST-83-15726. Portions of this work were done while L. M. held a National

Research Council–Naval Research Laboratory Research Associateship, and portions were taken from a thesis submitted in partial fulfillment of the requirements for the Ph.D. degree in the Department of Physics and Astronomy at the University of Maryland.

APPENDIX

OH MAIN-LINE ANOMALIES

The presence or absence of nonthermal excitation in the OH 18 cm hyperfine transitions affects the abundances and column densities derived in § IVb(ii) (i.e., Crutcher 1979, and references therein). The OH antenna temperatures for the core regions of the high-latitude molecular clouds are <0.1 K in all but three cases. Because most of the OH lines are very weak, it is difficult to obtain values of the antenna temperature and line width with 1σ errors less than 25% of the measured quantity. The 1σ errors in the antenna temperature ratio [$R \equiv T_A^*(1667)/T_A^*(1665)$] and integrated antenna temperature ratio [$R' \equiv \int T_A^*(1667)dv / \int T_A^*(1665)dv$] for the two main OH lines are large and they are shown in columns (3) and (5) of Table 6. Both R and R' must fall within the 1.0 (optically thick) to 1.8 (optically thin) range if OH is to be thermally excited; otherwise, the transitions are nonthermally excited and the line emission is said to be anomalous. Anomalies in the main-line emission may lead to errors in the OH column densities and may be present in all dark dust clouds (Crutcher 1979). Columns (2) and (4) of Table 6 present the values of R and of R' .

Although the signal-to-noise ratio of our observations is not large, we determine whether or not our data are consistent with thermal excitation. Only one line of sight out of 16 has a ratio R less than 1.0, while six lines of sight are greater than 1.8; for R' , no line of sight has a value less than 1.0, while the values for six lines of sight are greater than 1.8. Only cloud 40 possesses a line of sight which has values of R and R' greater than 1.8. The average R value is 1.60 with a 1σ standard deviation of 0.42, while the average R' value is 2.15 with a 1σ standard deviation of 1.74. If the two low-signal-to-noise velocity components in the second line of sight in cloud 55 are omitted from the data, the mean R' value is 1.61 with a standard deviation of 0.53. These results indicate that the OH emission is optically thin in the core regions of the high-latitude molecular clouds.

Let us assume that the lines of sight in our sample are all optically thin with values of R and R' equal to 1.8 and observations are randomly distributed about this value with a 1σ width characteristic of the uncertainties in R and R' . This width may be approximated by determining the mean of the 1σ errors in Table 6: ~ 0.5 for R and ~ 0.7 for R' . Consequently, for the R values in our sample, three values are expected to be greater than the mean value of 1.8 by more than 1 standard deviation. Similarly, excluding the two low-signal-to-noise components of cloud 55 in the R' data, two or three of the remaining values are expected to be greater than the mean by 1 standard deviation. One value of R and two values of R' are more than 1 standard deviation from 1.8; this indicates that the OH emission is consistent with thermal excitation. Although longer integration times are needed to firmly establish whether any main-line anomalies exist in these clouds, the OH emission, in general, is optically thin and thermally excited in the high-latitude clouds. Therefore, the abundances and column densities determined in § IVb(ii) should be unaffected by the anomalous excitation effects cited by Crutcher (1979).

REFERENCES

- Bachiller, R., and Cernicharo, J. 1986, *Astr. Ap.*, **166**, 283.
 Batrla, W., Walmsley, C. M., and Wilson, T. L. 1984, *Astr. Ap.*, **136**, 127.
 Bevington, P. R. 1969, *Data Reduction and Error Analysis for the Physical Sciences*, (New York: McGraw Hill).
 Blitz, L. 1987 in *Physical Processes in Interstellar Clouds*, ed. G. E. Morfill and M. Scholer (Dordrecht: Reidel), p. 35.
 Blitz, L., Magnani, L., and Wandel, A. 1987, *Ap. J.*, submitted.
 Bloemen, J. B. G. M., et al. 1984, *Astr. Ap.*, **139**, 37.
 ———, et al. 1986, *Astr. Ap.*, **154**, 25.
 Bohlin, R. C., Savage, B. D., and Drake, J. F. 1978, *Ap. J.*, **224**, 132.
 Chaffee, F. H., Jr., and Lutz, B. L. 1977, *Ap. J.*, **213**, 394.
 Cohen, R. J., Matthews, N., Few, R. W., and Booth, R. S. 1983, *M.N.R.A.S.*, **203**, 1123.
 Crutcher, R. M. 1977, *Ap. J.*, **216**, 308.
 ———, 1979, *Ap. J.*, **234**, 881.
 ———, 1980, *Ap. J.*, **239**, 549.
 Crutcher, R. M., and Watson, W. D. 1976, *Ap. J. (Letters)*, **203**, L123.
 de Vries, C. P. 1986, Ph.D. thesis, University of Leiden.
 de Vries, C. P., and Le Poole, R. S. 1985, *Astr. Ap.*, **145**, L7.
 de Vries, H. W., Heithausen, A., and Thaddeus, P. 1987, *Ap. J.*, **319**, 723.
 Dickman, R. L. 1975, *Ap. J.*, **202**, 50.
 ———, 1978a, *Ap. J. Suppl.*, **37**, 407.
 ———, 1978b, *A.J.*, **83**, 363.
 Dickman, R. L., and Clemens, D. P. 1983, *Ap. J.*, **271**, 143.
 Downes, D., Wilson, T. L., and Bieging, J. H. 1976, *Astr. Ap.*, **52**, 321.
 Draine, B. T. 1978, *Ap. J. Suppl.*, **36**, 595.
 Evans, N. J., II, and Kutner, M. L. 1976, *Ap. J.*, **204**, L131.
 Federman, S. R., Glassgold, A. E., Jenkins, E. B., and Shaya, E. J. 1980, *Ap. J.*, **242**, 545.
 Frerking, M. A., Langer, W. D., and Wilson, R. W. 1982, *Ap. J.*, **262**, 590.
 Glassgold, A. E., Huggins, P. J., and Langer, W. D. 1985, *Ap. J.*, **290**, 615, (GHL).
 Heiles, C. 1968, *Ap. J.*, **151**, 919.
 ———, 1969, *Ap. J.*, **157**, 123.
 ———, 1984, *Ap. J. Suppl.*, **55**, 585.
 Kazès, I., Crovisier, J., and Aubry, D. 1977, *Astr. Ap.*, **58**, 403.
 Knapp, G. R., and Kerr, F. J. 1973, *A.J.*, **78**, 453.
 Kutner, M. L. 1973, in *Molecules in the Galactic Environment*, ed. M. A. Gordon and L. E. Snyder (New York: Wiley and Sons), p. 199.
 Kutner, M. L., and Leung, C. M. 1985, *Ap. J.*, **291**, 188.
 Kutner, M. L., and Ulich, B. L. 1981, *Ap. J.*, **250**, 341.
 Lada, E. A., and Blitz, L. 1987, *Ap. J.*, in press.
 Lynds, B. T. 1962, *Ap. J. Suppl.*, **7**, 1.
 Magnani, L. 1987, Ph.D. thesis, University of Maryland.
 Magnani, L., Blitz, L., and Mundy, L. 1985, *Ap. J.*, **295**, 402, (MBM).
 Magnani, L., and de Vries, C. P. 1986, *Astr. Ap.*, **168**, 271.
 Mitchell, G. F., and Deveau, T. J. 1983, *Ap. J.*, **266**, 646.
 Myers, P. C. 1973, *Ap. J. Suppl.*, **26**, 83.
 ———, 1975, *Ap. J.*, **198**, 331.
 Myers, P. C., Ho, P. T. P., Schneps, M. H., Chin, G., Pankonin, V., and Winnberg, A. 1978, *Ap. J.*, **220**, 864.
 Nguyen-Q-Rieu, Winnberg, A., Guibert, J., Lepine, J. R. D., Johansson, L. E. B., and Goss, W. M. 1976, *Astr. Ap.*, **46**, 413.
 Penzias, A. A. 1980, *Science*, **208**, 663.
 Pöppel, W. G. L., Rohlf, K., and Celnik, W. 1983, *Astr. Ap.*, **126**, 152.
 Sancisi, R., Goss, W. M., Andersson, C., Johansson, L. E. B., and Winnberg, A. 1974, *Astr. Ap.*, **35**, 445.
 Savage, B. D., Bohlin, R. C., Drake, J. F., and Budich, W. 1977, *Ap. J.*, **216**, 291.
 Sherwood, W. A., and Wilson, T. L. 1981, *Astr. Ap.*, **101**, 72.
 Sume, A., Downes, D., and Wilson, T. L. 1975, *Astr. Ap.*, **39**, 435.

- Toriseva, M., and Mattila, K. 1985, *Astr. Ap.*, **153**, 207.
Turner, B. E. 1973, *Ap. J.*, **186**, 357.
Turner, B. E., and Heiles, C. 1971, *Ap. J.*, **170**, 453.
———. 1974, *Ap. J.*, **194**, 525.
van Dishoeck, E. F. and Black, J. H. 1986, *Ap. J. Suppl.*, **62**, 109.
———. 1987, in *Physical Processes in Interstellar Clouds*, ed. G. E. Morfill and M. Scholer (Dordrecht: Reidel), p. 241.
- Viala, Y. P. 1986, *Astr. Ap. Suppl.*, **64**, 391.
Williams, D. A. 1985, *Quart. J.R.A.S.*, **26**, 463.
Wouterloot, J. G. A. 1981, Ph. D. thesis, University of Leiden.
Young, J. S., Goldsmith, P. F., Langer, W. D., Wilson, R. W., and Carlson, E. R. 1982, *Ap. J.*, **261**, 513.

LEO BLITZ: Astronomy Program, University of Maryland, College Park, MD 20742

LORIS MAGNANI: Arecibo Observatory, P.O. Box 995, Arecibo, Puerto Rico 00613

JAN G. A. WOUTERLOOT: Max-Planck-Institut für Radioastronomie, Auf dem Hugel 69, D-5300, Bonn 1, FDR